

Electromagnetic nucleon-delta transition in the perturbative chiral quark model

K. Pumsa-ard, V. E. Lyubovitskij, Th. Gutsche, Amand Faessler
and S. Cheedket*

*Institut für Theoretische Physik, Universität Tübingen,
Auf der Morgenstelle 14, D-72076 Tübingen, Germany*

Abstract

We apply the perturbative chiral quark model to the $\gamma N \rightarrow \Delta$ transition. The four momentum dependence of the respective transverse helicity amplitudes $A_{1/2}$ and $A_{3/2}$ is determined at one loop in the pseudoscalar Goldstone boson fluctuations. Inclusion of excited states in the quark propagator is shown to result in a reasonable description of the experimental values for the helicity amplitudes at the real photon point.

PACS: 12.39.Ki, 13.40.Hq, 14.20.Gk,

Keywords: Chiral symmetry; Relativistic quark model; Effective Lagrangian; Helicity amplitudes.

*Present address: School of Physics, Institute of Science, Suranaree University of Technology, Nakhon Ratchasima 30000, Thailand

I. INTRODUCTION

Electromagnetic transitions of the nucleon to baryon excitations give important insight into the degrees of freedom which are relevant in hadron physics and hence for the structure of the nucleon. From this point of view the study of the particular transition $\gamma N \rightarrow \Delta(1232)$ is sensitive to the spatial and spin structure of the involved baryons.

A comparison between theory and experiment is conveniently performed on the level of electromagnetic transition matrix elements, which are expressed in terms of photon helicity amplitudes [1,2]. For transverse photons the electromagnetic $N - \Delta$ transition is described by the helicity amplitudes A_λ , where $\lambda = 3/2(1/2)$ refers to the case where the photon spin is parallel (antiparallel) to the spin of the nucleon target. In turn, the decay rate for $\Delta^+ \rightarrow p\gamma$ can be expressed in terms of these transverse helicity amplitudes [2,3]

$$\Gamma(\Delta^+ \rightarrow p\gamma) = \frac{(P^*)^2}{2\pi} \left(\frac{M_p}{M_\Delta} \right) \{|A_{1/2}|^2 + |A_{3/2}|^2\}, \quad (1)$$

where M_p and M_Δ are the baryon masses and

$$P^* = \frac{M_\Delta^2 - M_p^2}{2M_\Delta} = 258.4 \text{ MeV} \quad (2)$$

is the 3-momentum of either of the final state particles (proton or real photon) in the Δ -rest frame. Experimental values for the helicity amplitudes $A_{1/2}$ and $A_{3/2}$ at the real-photon point and for the branching ratio $\text{BR}(\Delta^+ \rightarrow p\gamma) = \Gamma(\Delta^+ \rightarrow p\gamma)/\Gamma_{total}(\Delta^+)$ are reported as [2]

$$\begin{aligned} A_{1/2} &= -(135 \pm 6) \times 10^{-3} \text{GeV}^{-1/2}, & A_{3/2} &= -(255 \pm 8) \times 10^{-3} \text{GeV}^{-1/2}, & (3) \\ \frac{A_{3/2}}{A_{1/2}} &= 1.89 \pm 0.10, & \text{BR}(\Delta^+ \rightarrow p\gamma) &= (0.52 - 0.60)\%. \end{aligned}$$

Alternatively, the transverse helicity amplitudes can be expressed in terms of electromagnetic production multipoles, that is the magnetic dipole $M1$ and the electric quadrupole $E2$ moments. The two sets of amplitudes are related by

$$A_{1/2} = -\frac{1}{2}(M1 + 3E2), \quad A_{3/2} = -\frac{\sqrt{3}}{2}(M1 - E2). \quad (4)$$

Thereby, a non-vanishing $E2/M1$ ratio indicates the possibility of an intrinsic deformation of the nucleon [4–6] or a contribution from meson exchange currents [7,8] with the latest experimental value of [2]

$$\frac{E2}{M1} = -0.025 \pm 0.005. \quad (5)$$

Various model calculations have been applied to the transverse helicity amplitudes of the electromagnetic $N \rightarrow \Delta$ transition. In the original constituent quark model [1,9,10] the results for the helicity amplitudes at the real-photon point are somewhat smaller than the experimental data. Further extensions of the constituent quark model by considering

two-body currents based on gluon and exchange were performed in [7,8]. However, in these calculations lower values for the $M1$ contribution as compared to the experimental ones are still obtained even when also including relativistic effects. In the cloudy bag model [11–13] this situation was improved where pion cloud corrections are shown to contribute up to two thirds of the total amplitude. Similar models, e.g., the relativistic potential quark model [14], confirmed the importance of meson cloud corrections. In these model calculations one is also able to generate a non-vanishing value for the $E2/M1$ ratio, which is extremely sensitive to non-valence quark degrees of freedom, referred to as the pion cloud of the nucleon or as exchange currents. With the exception of Ref. [7], predictions for this ratio are usually considerably smaller than the experimental value of Eq. (5).

As a further development of chiral quark models with a perturbative treatment of the Goldstone boson cloud [15]- [17] we recently developed the perturbative chiral quark model (PCQM) for the description of low-energy properties of baryons [18]- [22]. The PCQM is based on the nonlinear σ -model quark Lagrangian and includes a phenomenological confinement potential. Baryons are considered as bound states of valence quarks surrounded by a cloud of pseudoscalar mesons as imposed by chiral symmetry requirements. The model was successfully applied to the electromagnetic properties of the nucleon [19], σ -term physics [20], the πN scattering including radiative corrections [21] and the strange nucleon form factors [22].

In the current work we consider, as a further extension, the determination of the momentum dependence of the helicity amplitudes $A_{1/2}$ and $A_{3/2}$ of the $N - \Delta$ transition at one-loop or equivalently to the order of accuracy $o(1/F^2, \hat{m}, m_s)$. Here, F is the pion decay constant in the chiral limit and \hat{m}, m_s are the respective current masses of up/down and strange quarks. In the context of the current approach we furthermore investigate the role of excited quark states in meson loop diagrams. Whereas in our previous considerations the expansion of the quark propagator was restricted to include only ground state contributions, that is N and Δ intermediate states in loop diagrams, we now also consider excited quark states. The main conclusion drawn from this calculation will be that inclusion of excited quark states are relevant at the 20% level in order to obtain a reasonable description of the transverse helicity amplitudes at the real-photon point. For the $E2/M1$ ratio we trivially obtain a vanishing value, since at the order of accuracy we are working in a non-vanishing result cannot be expected due to large- N_c QCD arguments [3].

In the present article we proceed as follows. In the following section we review the basic notions of the perturbative chiral quark model and the modifications of the perturbative technique when including the full quark propagator. In Sec. III we present the calculation of the transverse $N - \Delta$ helicity amplitudes and give a comparison with current experimental data. Finally, Sec.IV contains a summary of our major conclusions.

II. THE PERTURBATIVE CHIRAL QUARK MODEL (PCQM)

The starting point of the perturbative chiral quark model [18]- [22] is an effective chiral Lagrangian describing the valence quarks of baryons as relativistic fermions moving in an external field (static potential) $V_{\text{eff}}(r) = S(r) + \gamma^0 V(r)$ with $r = |\vec{x}|$ [18,19], which in the SU(3)-flavor version are supplemented by a cloud of Goldstone bosons (π, K, η). Treating

Goldstone fields as small fluctuations around the three-quark (3q) core we have the linearized effective Lagrangian [19]:

$$\begin{aligned} \mathcal{L}_{\text{eff}}(x) = & \bar{\psi}(x)[i \not{\partial} - S(r) - \gamma^0 V(r)]\psi(x) + \frac{1}{2}[\partial_\mu \hat{\Phi}(x)]^2 \\ & - \bar{\psi}(x)S(r)i\gamma^5 \frac{\hat{\Phi}(x)}{F}\psi(x) + \mathcal{L}_{\chi SB}(x). \end{aligned} \quad (6)$$

The additional term $\mathcal{L}_{\chi SB}$ contains the mass contributions both for quarks and mesons, which explicitly break chiral symmetry:

$$\mathcal{L}_{\chi SB}(x) = -\bar{\psi}(x)\mathcal{M}\psi(x) - \frac{B}{2}Tr[\hat{\Phi}^2(x)\mathcal{M}]. \quad (7)$$

Here, $\hat{\Phi}$ is the octet matrix of pseudoscalar mesons

$$\frac{\hat{\Phi}}{\sqrt{2}} = \begin{pmatrix} \pi^0/\sqrt{2} + \eta/\sqrt{6} & \pi^+ & K^+ \\ \pi^- & -\pi^0/\sqrt{2} + \eta/\sqrt{6} & K^0 \\ K^- & \bar{K}^0 & -2\eta/\sqrt{6} \end{pmatrix}, \quad (8)$$

$F = 88$ MeV is the pion decay constant in the chiral limit [23], $\mathcal{M} = \text{diag}\{\hat{m}, \hat{m}, m_s\}$ is the mass matrix of current quarks (we restrict to the isospin symmetry limit $m_u = m_d = \hat{m}$) and $B = -\langle 0|\bar{u}u|0 \rangle / F^2$ is the quark condensate constant. We rely on the standard picture of chiral symmetry breaking [24] and for the masses of pseudoscalar mesons we use the leading term in their chiral expansion (i.e. linear in the current quark mass):

$$M_\pi^2 = 2\hat{m}B, \quad M_K^2 = (\hat{m} + m_s)B, \quad M_\eta^2 = \frac{2}{3}(\hat{m} + 2m_s)B. \quad (9)$$

The following set of parameters [24] is chosen in our evaluation

$$\hat{m} = 7 \text{ MeV}, \quad \frac{m_s}{\hat{m}} = 25, \quad B = \frac{M_{\pi^+}^2}{2\hat{m}} = 1.4 \text{ GeV}. \quad (10)$$

Meson masses obtained in Eq. (9) satisfy the Gell-Mann-Oakes-Renner and the Gell-Mann-Okubo relation. In addition, the linearized effective Lagrangian in Eq. (6) fulfils the PCAC requirement.

We expand the quark field ψ in the basis of potential eigenstates as

$$\psi(x) = \sum_\alpha b_\alpha u_\alpha(\vec{x}) \exp(-i\mathcal{E}_\alpha t) + \sum_\beta d_\beta^\dagger v_\beta(\vec{x}) \exp(i\mathcal{E}_\beta t),$$

where the sets of quark $\{u_\alpha\}$ and antiquark $\{v_\beta\}$ wave functions in orbits α and β are solutions of the Dirac equation with the static potential $V_{\text{eff}}(r)$. The expansion coefficients b_α and d_β^\dagger are the corresponding single quark annihilation and antiquark creation operators.

We formulate perturbation theory in the expansion parameter $1/F$ ($F \sim \sqrt{N_c}$) and treat finite current quark masses perturbatively [19]. All calculations are performed at one loop or at order of accuracy $o(1/F^2, \hat{m}, m_s)$. In the calculation of matrix elements we project quark diagrams on the respective baryon states. The baryon states are conventionally set up by the

product of the SU(6) spin-flavor and SU(3)_c color wave functions, where the nonrelativistic single quark spin wave function is replaced by the relativistic solution $u_\alpha(\vec{x})$ of the Dirac equation

$$\left[-i\gamma^0\vec{\gamma}\cdot\vec{\nabla} + \gamma^0S(r) + V(r) - \mathcal{E}_\alpha\right]u_\alpha(\vec{x}) = 0, \quad (11)$$

where \mathcal{E}_α is the single-quark energy.

For the description of baryon properties we use the effective potential $V_{\text{eff}}(r)$ with a quadratic radial dependence [19,20]:

$$S(r) = M_1 + c_1r^2, \quad V(r) = M_2 + c_2r^2 \quad (12)$$

with the particular choice

$$M_1 = \frac{1 - 3\rho^2}{2\rho R}, \quad M_2 = \mathcal{E}_0 - \frac{1 + 3\rho^2}{2\rho R}, \quad c_1 \equiv c_2 = \frac{\rho}{2R^3}. \quad (13)$$

Here, \mathcal{E}_0 is the single-quark ground-state energy; R and ρ are parameters related to the ground-state quark wave function u_0 :

$$u_0(\vec{x}) = N_0 \exp\left[-\frac{\vec{x}^2}{2R^2}\right] \begin{pmatrix} 1 \\ i\rho\vec{\sigma}\vec{x}/R \end{pmatrix} \chi_s \chi_f \chi_c, \quad (14)$$

where $N_0 = [\pi^{3/2}R^3(1 + 3\rho^2/2)]^{-1/2}$ is a normalization constant; χ_s , χ_f , χ_c are the spin, flavor and color quark wave function, respectively. Note, that the constant part of the scalar potential M_1 can be interpreted as the constituent mass of the quark, which is simply the displacement of the current quark mass due to the potential $S(r)$. The parameter ρ is related to the axial charge g_A of the nucleon calculated in zeroth-order (or 3q-core) approximation:

$$g_A = \frac{5}{3} \left(1 - \frac{2\rho^2}{1 + \frac{3}{2}\rho^2}\right). \quad (15)$$

Therefore, ρ can be replaced by g_A using the matching condition (15). The parameter R is related to the charge radius of the proton in the zeroth-order approximation as

$$\langle r_E^2 \rangle_{LO}^P = \int d^3x u_0^\dagger(\vec{x}) \vec{x}^2 u_0(\vec{x}) = \frac{3R^2}{2} \frac{1 + \frac{5}{2}\rho^2}{1 + \frac{3}{2}\rho^2}. \quad (16)$$

In our calculations we use the value $g_A=1.25$ [19]. Therefore, we have only one free parameter, that is R . In the numerical studies [19] R is varied in the region from 0.55 fm to 0.65 fm, which corresponds to a change of $\langle r_E^2 \rangle_{LO}^P$ from 0.5 to 0.7 fm².

The expectation value of an operator \hat{A} is set up as:

$$\langle \hat{A} \rangle^B = {}^B\langle \phi_0 | \sum_{n=1}^{\infty} \frac{i^n}{n!} \int d^4x_1 \dots \int d^4x_n T[\mathcal{L}_I(x_1) \dots \mathcal{L}_I(x_n) \hat{A}] | \phi_0 \rangle_c^B, \quad (17)$$

where the state vector $|\phi_0\rangle$ corresponds to the unperturbed three-quark state (3q-core). Superscript “B” in (17) indicates that the matrix elements have to be projected onto the

respective baryon states, whereas subscript “*c*” refers to contributions from connected graph only. $\mathcal{L}_I(x)$ of Eq. (17) refers to the linearized quark-meson interaction Lagrangian:

$$\mathcal{L}_I(x) = -\bar{\psi}(x)i\gamma^5\frac{\hat{\Phi}(x)}{F}S(r)\psi(x). \quad (18)$$

For the evaluation of Eq.(17) we apply Wick’s theorem with the appropriate propagators for quarks and mesons.

For the quark field we use a Feynman propagator for a fermion in a binding potential with

$$\begin{aligned} iG_\psi(x, y) &= \langle \phi_0 | T \{ \psi(x) \bar{\psi}(y) \} | \phi_0 \rangle \\ &= \theta(x_0 - y_0) \sum_{\alpha} u_{\alpha}(\vec{x}) \bar{u}_{\alpha}(\vec{y}) e^{-i\mathcal{E}_{\alpha}(x_0 - y_0)} - \theta(y_0 - x_0) \sum_{\beta} v_{\beta}(\vec{x}) \bar{v}_{\beta}(\vec{y}) e^{i\mathcal{E}_{\beta}(x_0 - y_0)}. \end{aligned} \quad (19)$$

In previous applications [19]- [22] we restricted the expansion of the quark propagator to its ground state with:

$$iG_\psi(x, y) \rightarrow iG_0(x, y) \doteq u_0(\vec{x}) \bar{u}_0(\vec{y}) e^{-i\mathcal{E}_0(x_0 - y_0)} \theta(x_0 - y_0). \quad (20)$$

Such a truncation can be considered as an additional regularization of the quark propagator, where in the case of SU(2)-flavor intermediate baryon states in loop-diagrams are restricted to N and Δ . In the current approach we also include, for the first time, excited quark states in the propagator of Eq. (19) and analyse their influence on the matrix elements for the N - Δ transitions considered. We include the following set of excited quark states: the first p -states ($1p_{1/2}$ and $1p_{3/2}$ in the non-relativistic notation) and the second excited states ($1d_{3/2}$, $1d_{5/2}$ and $2s_{1/2}$). For the given form of the effective potential (12) the Dirac equation can be solved analytically. The corresponding expressions for the wave functions of the excited quark states are given in the Appendix. For the meson fields we adopt the free Feynman propagator with

$$i\Delta_{ij}(x - y) = \langle 0 | T \{ \Phi_i(x) \Phi_j(y) \} | 0 \rangle = \delta_{ij} \int \frac{d^4k}{(2\pi)^4} \frac{\exp[-ik(x - y)]}{i(M_{\Phi}^2 - k^2 - i\epsilon)}. \quad (21)$$

Introduction of the electromagnetic field A_{μ} to the effective Lagrangian (6) is accomplished by minimal substitution:

$$\partial_{\mu}\psi \rightarrow D_{\mu}\psi = \partial_{\mu}\psi + ieQA_{\mu}\psi, \quad \partial_{\mu}\Phi_i \rightarrow D_{\mu}\Phi_i = \partial_{\mu}\Phi_i + e\left[f_{3ij} + \frac{f_{8ij}}{\sqrt{3}}\right]A_{\mu}\Phi_j \quad (22)$$

where $Q = \text{diag}\{2/3, -1/3, -1/3\}$ is the quark charge matrix and f_{ijk} are the totally anti-symmetric structure constants of $SU(3)$. For the photon field A_{μ} we also include the usual kinetic term

$$\mathcal{L}_{ph} = -\frac{1}{4}F_{\mu\nu}(x)F^{\mu\nu}(x) \quad \text{with} \quad F_{\mu\nu}(x) = \partial_{\nu}A_{\mu}(x) - \partial_{\mu}A_{\nu}(x). \quad (23)$$

In the evaluation of Eq. (17) we redefine the perturbation series in terms of renormalized quantities, where a set of counterterms $\delta\mathcal{L}$ has to be introduced in the Lagrangian (6). The

counterterms play a dual role: i) they maintain the proper definition of physical parameters, such as nucleon mass and, in particular, the nucleon charge and ii) they effectively reduce the number of Feynman diagrams to be evaluated. For a detailed derivation and discussion of this renormalization technique see the original reference [19]. Here we just indicate the relevant results following the technique of Ref. [19], where now intermediate excited quark states are included in the loop diagrams. In the following we attach the index “0” to quantities when we truncate the quark propagator to the ground state contribution, index “F” refers to the case where excited states are also included.

First we introduce the renormalized quark field $\psi^r(x)$, which is a solution to the Dirac equation (11) with the full, renormalized non-strange quark mass [19]

$$\hat{m}_F^r = \hat{m} - \sum_{\alpha} \frac{1}{3\gamma} \left(\frac{1}{\pi F} \right)^2 \int_0^{\infty} dp p^2 F_{\alpha}(p^2) F_{\alpha}^{\dagger}(p^2) \left\{ \frac{9}{4} \mathcal{C}_{\alpha}^{\pi}(p^2) + \frac{3}{2} \mathcal{C}_{\alpha}^K(p^2) + \frac{1}{4} \mathcal{C}_{\alpha}^{\eta}(p^2) \right\}, \quad (24)$$

including self-energy corrections of the meson cloud. In Eq. (24) we introduce the relativistic reduction factor $\gamma = (1 - \frac{3}{2}\rho^2)/(1 + \frac{3}{2}\rho^2)$ and

$$\mathcal{C}_{\alpha}^{\phi}(p^2) = \frac{1}{w_{\phi}(p^2)(w_{\phi}(p^2) + \Delta\mathcal{E}_{\alpha})} \quad (25)$$

with meson energy $w_{\phi}(p^2) = \sqrt{M_{\phi}^2 + p^2}$ and momentum $p = |\vec{p}|$. $\Delta\mathcal{E}_{\alpha} = \mathcal{E}_{\alpha} - \mathcal{E}_0$ is the excess of the energy of the quark in state α with respect to the ground state. At the quark-meson vertex we obtain the form factor for the transition from a quark in the ground state to an excited one ($\alpha = (nljm)$) with

$$F_{\alpha}(p^2) = N_0 N_{\alpha} \frac{\partial}{\partial p} \int_0^{\infty} dr r S(r) (g_0(r) f_{\alpha}(r) + g_{\alpha}(r) f_0(r)) \\ \times \int_{\Omega} d\cos\theta d\phi e^{i p r \cos\theta} C_{\alpha} Y_{l_0}(\theta, \phi) \quad (26)$$

with $C_{\alpha} \doteq (l_0 \frac{1}{2} \frac{1}{2} |j \frac{1}{2})$. Explicit forms of the radial wave functions (g_{α} and f_{α}), normalizations (N_{α}) and energy difference ($\Delta\mathcal{E}_{\alpha}$) are given in the Appendix. When the quark propagator is restricted to the ground state only, the renormalized quark mass reduces to [19]

$$\hat{m}_0^r = \hat{m} - \frac{1}{3\gamma} \frac{9}{400} \left(\frac{g_A}{\pi F} \right)^2 \int_0^{\infty} dp p^4 F_{\pi NN}^2(p^2) \left\{ \frac{9}{w_{\pi}^2(p^2)} + \frac{6}{w_K^2(p^2)} + \frac{1}{w_{\eta}^2(p^2)} \right\}, \quad (27)$$

where $F_{\pi NN}(p^2)$ is the πNN form factor normalized to unity at zero recoil ($p^2 = 0$):

$$F_{\pi NN}(p^2) = \exp\left(-\frac{p^2 R^2}{4}\right) \left\{ 1 + \frac{p^2 R^2}{8} \left(1 - \frac{5}{3g_A} \right) \right\}. \quad (28)$$

For the effective potential considered the relationship between renormalized and bare potential eigenstates can be deduced analytically.

When the original Lagrangian (6) is rewritten in terms of renormalized quark fields and masses, a set of counterterms, denoted by $\delta\mathcal{L}^{str}$, has to be included:

$$\begin{aligned}\delta\mathcal{L}^{str} &= \delta\mathcal{L}_1^{str} + \delta\mathcal{L}_2^{str} + \delta\mathcal{L}_3^{str}, \\ \text{with} \\ \delta\mathcal{L}_1^{str} &= \bar{\psi}^r(x) (Z - 1) [i \not{\partial} - \mathcal{M}^r - S(r) - \gamma^0 V(r)] \psi^r(x), \\ \delta\mathcal{L}_2^{str} &= -\bar{\psi}^r(x) \delta\mathcal{M} \psi^r(x), \\ \delta\mathcal{L}_3^{str} &= -c_\pi \sum_{i=1}^3 [\bar{\psi}^r(x) i\gamma^5 \lambda_i \psi^r(x)]^2 - c_K \sum_{i=4}^7 [\bar{\psi}^r(x) i\gamma^5 \lambda_i \psi^r(x)]^2 - c_\eta [\bar{\psi}^r(x) i\gamma^5 \lambda_8 \psi^r(x)]^2. \quad (29)\end{aligned}$$

In the counterterms \mathcal{M}^r is the mass matrix of renormalized quark masses and $\mathcal{M}^r = \mathcal{M} - \delta\mathcal{M}$. The terms in $\delta\mathcal{L}_3^{str}$ are introduced for the purpose of nucleon mass renormalization due to meson exchange between different quarks and contain the factors

$$c_\Phi = -\frac{9}{200} \frac{(2\pi R^2)^{3/2}}{(1 - \gamma^2)} \Pi(M_\Phi^2) \quad \text{with} \quad \Pi(M_\Phi^2) = -\left(\frac{g_A}{\pi F}\right)^2 \int_0^\infty \frac{dp p^4}{w_\Phi^2(p^2)} F_{\pi NN}^2(p^2). \quad (30)$$

The renormalization constants \hat{Z} for u, d -quarks and Z_s for the s -quark are given in the diagonal matrix $Z = \text{diag}\{\hat{Z}, \hat{Z}, Z_s\}$. The values of \hat{Z} and Z_s are determined by the charge conservation condition at one loop [19]. Due to the consistency of our approach the values of \hat{Z} and Z_s guarantee charge conservation both on the quark and the baryon level. In the context of the present calculation we only have to consider the renormalization constant \hat{Z} for the non-strange quarks. When excited quark states are included we obtain the following analytical expression for the renormalization constant

$$\hat{Z}^F = 1 - \sum_\alpha \left(\frac{1}{\pi F}\right)^2 \int_0^\infty dp p^2 F_\alpha(p^2) F_\alpha^\dagger(p^2) \left\{ \frac{3}{4} \mathcal{W}_\alpha^\pi(p^2) + \frac{1}{2} \mathcal{W}_\alpha^K(p^2) + \frac{1}{12} \mathcal{W}_\alpha^\eta(p^2) \right\} \quad (31)$$

with

$$\mathcal{W}_\alpha^\phi(p^2) = \frac{1}{w_\phi(p^2)(w_\phi(p^2) + \Delta\mathcal{E}_\alpha)^2}. \quad (32)$$

When we restrict intermediate quark states to the ground state, the expression of Eq.(31) reduces to

$$\hat{Z}^0 = 1 - \frac{27}{400} \left(\frac{g_A}{\pi F}\right)^2 \int_0^\infty dp p^4 F_{\pi NN}^2(p^2) \left\{ \frac{1}{w_\pi^3(p^2)} + \frac{2}{3w_K^3(p^2)} + \frac{1}{9w_\eta^3(p^2)} \right\}. \quad (33)$$

which has already been derived in [19]. In the two-flavor picture, that is when we restrict to the pion cloud contribution only, we obtain a value of $\hat{Z}^0 = 0.9 \pm 0.02$ for our set of parameters. The contribution of kaon and η -meson loops to the constant \hat{Z}^0 is strongly suppressed due to the energy denominators in Eq. (33). In the three-flavor picture we get $\hat{Z}^0 = 0.88 \pm 0.03$, which deviates only slightly from the two-flavor result. With the value for

\hat{Z}^0 being close to unity, for our set of parameters the perturbative treatment of the meson cloud is also justified. Inclusion of the excited states changes the value of the renormalization constant to $\hat{Z}^F = 0.81 \pm 0.04$.

For the $N \rightarrow \Delta$ transition we use the renormalized electromagnetic current operator j_r^μ as derived by Noether's theorem [19]:

$$j_r^\mu = j_{\psi^r}^\mu + j_\Phi^\mu + \delta j_{\psi^r}^\mu. \quad (34)$$

It contains the quark component $j_{\psi^r}^\mu$, the charged meson component j_Φ^μ and the contribution of the counterterm $\delta j_{\psi^r}^\mu$:

$$j_{\psi^r}^\mu = \bar{\psi}^r \gamma^\mu Q \psi^r \equiv \frac{1}{3} [2 \bar{u}^r \gamma^\mu u^r - \bar{d}^r \gamma^\mu d^r - \bar{s}^r \gamma^\mu s^r], \quad (35)$$

$$j_\Phi^\mu = \left[f_{3ij} + \frac{f_{8ij}}{\sqrt{3}} \right] \Phi_i \partial^\mu \Phi_j \equiv [\pi^- i \partial^\mu \pi^+ - \pi^+ i \partial^\mu \pi^- + K^- i \partial^\mu K^+ - K^+ i \partial^\mu K^-],$$

and

$$\delta j_{\psi^r}^\mu = \bar{\psi}^r (Z - 1) \gamma^\mu Q \psi^r \equiv \frac{1}{3} [2 (\hat{Z} - 1) \bar{u}^r \gamma^\mu u^r - (\hat{Z} - 1) \bar{d}^r \gamma^\mu d^r - (Z_s - 1) \bar{s}^r \gamma^\mu s^r].$$

Again, further technical details of the presented formalism are contained in the original reference [19], but here it is extended to the case where excited states are included in the quark propagator.

III. $\gamma N \rightarrow \Delta$ HELICITY AMPLITUDES IN THE PCQM

Now we consider the determination of the helicity amplitudes for the transition $\gamma N \rightarrow \Delta$ in the PCQM. The transverse helicity amplitudes are defined as

$$A_M = -\frac{e}{\sqrt{2\omega_\gamma}} \langle \Delta, s'_z = M | \vec{j} \cdot \vec{\epsilon} | N, s_z = M - 1 \rangle \quad (36)$$

where $M = \frac{1}{2}, \frac{3}{2}$ and $\omega_\gamma \equiv P^* = (M_\Delta^2 - M_N^2)/2M_\Delta$ is the energy of the photon in the rest frame of the Δ with the polarization vector $\vec{\epsilon}$; M_N and M_Δ are the physical masses of the nucleon and the $\Delta(1232)$ -resonance, respectively.

In the PCQM the helicity amplitudes $A_{1/2}(q^2)$ and $A_{3/2}(q^2)$, where q is the photon four-momentum with $Q^2 = -q^2$, are then identified with the perturbative expressions:

$$A_{1/2}(Q^2) = -\frac{e}{\sqrt{2\omega_\gamma}} \langle \Delta^+, 1/2 | -\frac{1}{2} \int \delta(t) d^4x d^4x_1 d^4x_2 e^{-iqx} \\ \times T[\mathcal{L}_{str}^r(x_1) \mathcal{L}_{str}^r(x_2) \vec{j}_r(x) \cdot \vec{\epsilon}] | p, -1/2 \rangle_c, \quad (37)$$

$$A_{3/2}(Q^2) = -\frac{e}{\sqrt{2\omega_\gamma}} \langle \Delta^+, 3/2 | -\frac{1}{2} \int \delta(t) d^4x d^4x_1 d^4x_2 e^{-iqx} \\ \times T[\mathcal{L}_{str}^r(x_1) \mathcal{L}_{str}^r(x_2) \vec{j}_r(x) \cdot \vec{\epsilon}] | p, 1/2 \rangle_c, \quad (38)$$

where $|B, M \rangle \doteq |\phi_0 \rangle^{B_M}$ refers to the unperturbed three-quark state of baryon B with spin projection M. Here, \vec{j}_r is the spatial part of the renormalized electromagnetic current

operator already introduced in Eq. (34). $\mathcal{L}_{str}^r = \mathcal{L}_I^{str} + \delta\mathcal{L}^{str}$ is the renormalized strong interaction Lagrangian [19] containing the quark-meson interaction term

$$\mathcal{L}_I^{str} = -\bar{\psi}^r(x) i\gamma^5 \frac{\hat{\Phi}(x)}{F} S(r) \psi^r(x) \quad (39)$$

and the set of counterterms $\delta\mathcal{L}^{str}$ of Eq. (29).

The helicity amplitudes $A_{1/2}$ and $A_{3/2}$ are evaluated at one-loop or to the order of accuracy $o(1/F^2, \hat{m}, m_s)$. At this level, which is also equivalent to $O(1/N_c)$ as will be discussed later, we obtain the naive relation $A_{3/2} = \sqrt{3} \cdot A_{1/2}$, which can also be checked explicitly. Therefore, in the following we only present explicit analytical results for the helicity amplitude $A_{1/2}$.

We start with the simplest case, where the quark propagator is restricted to the ground state contribution. The total helicity amplitude is a sum of terms arising from different diagrams: the three-quark diagram (Fig.1a), the counterterm (Fig.1b), the meson-cloud diagram (Fig.1c), the vertex-correction diagram (Fig.1d) and the meson-in-flight diagram (Fig.1e).

(a) The helicity amplitude due to the three-quark diagram [Fig.1(a)] is given by a leading order (LO) and a next-to-leading (NLO) term, where the latter one arises after renormalization [19]:

$$A_{1/2}(Q^2) \Big|_{3q} = A_{1/2}(Q^2) \Big|_{3q}^{LO} + A_{1/2}(Q^2) \Big|_{3q}^{NLO} \quad (40)$$

$$A_{1/2}(Q^2) \Big|_{3q}^{LO} = -\frac{2}{3} \frac{e P^*(Q^2)}{\sqrt{2\omega_\gamma}} \rho R \frac{\exp\left(-\frac{Q^2 R^2}{4}\right)}{1 + \frac{3\rho^2}{2}} \quad (41)$$

$$A_{1/2}(Q^2) \Big|_{3q}^{NLO} = A_{1/2}(Q^2) \Big|_{3q}^{LO} \hat{m}_0^r \left(\frac{\rho R}{1 + \frac{3\rho^2}{2}} \right) \left(\frac{Q^2 R^2}{4} - \frac{2 - \frac{3\rho^2}{2}}{1 + \frac{3\rho^2}{2}} \right). \quad (42)$$

The absolute value of the 3-momentum

$$P^*(Q^2) = \frac{\sqrt{(M_\Delta^2 - M_N^2 - Q^2)^2 + 4 M_\Delta^2 Q^2}}{2M_\Delta} \quad (43)$$

of either the nucleon or the virtual photon is evaluated in the Δ -rest frame.

(b) The three-quark counterterm (CT) [Fig.1(b)] results in the expression:

$$A_{1/2}(Q^2) \Big|_{CT} = (\hat{Z}^0 - 1) A_{1/2}(Q^2) \Big|_{3q}^{LO}. \quad (44)$$

(c) The meson-cloud diagram (MC) [Fig.1(c)] yields:

$$\begin{aligned} A_{1/2}(Q^2) \Big|_{MC} &= -\frac{3}{200} \frac{e P^*(Q^2)}{\sqrt{2\omega_\gamma}} \left(\frac{g_A}{\pi F} \right)^2 \int_0^\infty dp p^4 \int_{-1}^1 dx (1-x^2) \\ &\times \mathcal{F}_{\pi NN}(p^2, Q^2, x) t_N(p^2, Q^2, x) \Big|_{MC}, \end{aligned} \quad (45)$$

where

$$\begin{aligned}
\mathcal{F}_{\pi NN}(p^2, Q^2, x) &= F_{\pi NN}(p^2)F_{\pi NN}(p_+^2), \\
t_N(p^2, Q^2, x) \Big|_{MC} &= 2D_\pi(p^2, Q^2, x) + D_K(p^2, Q^2, x), \\
D_\Phi(p^2, Q^2, x) &= \frac{1}{w_\Phi^2(p^2)w_\Phi^2(p_+^2)}, \\
p_\pm^2 &= p^2 + Q^2 \pm 2p\sqrt{Q^2}x.
\end{aligned} \tag{46}$$

(d) For the vertex-correction diagram (VC) [Fig.1(d)] we obtain:

$$\begin{aligned}
A_{1/2}(Q^2) \Big|_{VC} &= -\frac{1}{200} \frac{e P^*(Q^2)}{\sqrt{2\omega_\gamma}} \left(\frac{g_A}{\pi F} \right)^2 \exp\left(-\frac{Q^2 R^2}{4} \right) \frac{\rho R}{1 + \frac{3\rho^2}{2}} \\
&\times \int_0^\infty dp p^4 F_{\pi NN}^2(p^2) t_N(p^2) \Big|_{VC}
\end{aligned} \tag{47}$$

where

$$\begin{aligned}
t_N(p^2) \Big|_{VC} &= W_\pi(p^2) - \frac{1}{3}W_\eta(p^2), \\
W_\Phi(p^2) &= \frac{1}{w_\Phi^3(p^2)}.
\end{aligned} \tag{48}$$

(e) And for the meson-in-flight diagram (MF) [Fig.1(e)] we get:

$$\begin{aligned}
A_{1/2}(Q^2) \Big|_{MF} &= -\frac{9}{200} \frac{e P^*(Q^2)}{\sqrt{2\omega_\gamma}} \left(\frac{g_A}{\pi F} \right)^2 \int_0^\infty dp p^4 \int_{-1}^1 dx (1-x^2) \\
&\times \mathcal{F}_{\pi NN}(p^2, Q^2, x) D_\pi(p^2, Q^2, x).
\end{aligned} \tag{49}$$

When including excited states in the quark propagator, the analytical results for the LO three-quark diagram and the meson-in-flight contribution obviously still remain the same. In turn the following contributions must be extended.

(a) In the three-quark NLO expression the renormalized quark mass has to be replaced accordingly

$$A_{1/2}(Q^2) \Big|_{3q}^{NLO} = A_{1/2}(Q^2) \Big|_{3q}^{LO} \hat{m}_F^r \left(\frac{\rho R}{1 + \frac{3\rho^2}{2}} \right) \left(\frac{Q^2 R^2}{4} - \frac{2 - \frac{3\rho^2}{2}}{1 + \frac{3\rho^2}{2}} \right). \tag{50}$$

(b) For the three-quark counterterm (CT) the appropriate renormalization constant has to be inserted

$$A_{1/2}(Q^2) \Big|_{CT} = (\hat{Z}^F - 1) A_{1/2}(Q^2) \Big|_{3q}^{LO}. \tag{51}$$

(c) For the meson-cloud diagram (MC) we obtain the full expression

$$A_{1/2}(Q^2)\Big|_{MC} = -\frac{1}{6} \frac{e P^*(Q^2)}{\sqrt{2\omega_\gamma}} \left(\frac{1}{\pi F}\right)^2 \int_0^\infty dp p^3 \int_{-1}^1 dx \frac{1-x^2}{\sqrt{p_+^2}} \\ \times \sum_\alpha \mathcal{F}_{\alpha;MC}(p^2, Q^2, x) t(p^2, Q^2, x)\Big|_{\alpha;MC}$$

where the sum runs over the index α , labelling the quantum numbers of the intermediate quark states (ground and excited states). We use the definitions

$$t(p^2, Q^2, x)\Big|_{\alpha;MC} = 2\mathcal{D}_\alpha^\pi(p^2, Q^2, x) + \mathcal{D}_\alpha^K(p^2, Q^2, x) \quad (52)$$

and

$$\mathcal{D}_\alpha^\phi = \frac{1 + [\Delta\mathcal{E}_\alpha/(w_\phi(p_+^2) + w_\phi(p^2))]}{w_\phi(p^2)w_\phi(p_+^2)(w_\phi(p^2) + \Delta\mathcal{E}_\alpha)(w_\phi(p_+^2) + \Delta\mathcal{E}_\alpha)}, \quad (53)$$

where in addition we introduce the function $\mathcal{F}_{\alpha;MC}(p^2, Q^2, x) = F_\alpha(p_+^2)F_\alpha^\dagger(p^2)$ with the vertex form factor $F_\alpha(p^2)$ of Eq. (26).

(d) For the vertex-correction diagram (VC) inclusion of excited states results in

$$A_{1/2}(Q^2)\Big|_{VC} = \sum_{\beta,\alpha} \frac{I_{\beta\alpha}(Q^2)}{18} \frac{e P^*(Q^2)}{\sqrt{2\omega_\gamma}} \left(\frac{1}{\pi F}\right)^2 \int_0^\infty dp p^2 \mathcal{F}_{\beta\alpha;VC}(p^2) t(p^2)\Big|_{\beta\alpha;VC}, \quad (54)$$

where

$$t(p^2)\Big|_{\beta\alpha;VC} = \mathcal{W}_{\beta\alpha}^\pi(p^2) - \frac{1}{3}\mathcal{W}_{\beta\alpha}^\eta(p^2), \quad (55)$$

$$\mathcal{W}_{\beta\alpha}^\phi(p^2) = \frac{1}{w_\phi(p^2)(w_\phi(p^2) + \Delta\mathcal{E}_\beta)(w_\phi(p^2) + \Delta\mathcal{E}_\alpha)} \quad (56)$$

and $\mathcal{F}_{\beta\alpha;VC} = F_\beta(p^2)F_\alpha^\dagger(p^2)$. We also define

$$I_{\beta\alpha}(Q^2) = 2N_\beta N_\alpha \frac{\partial}{\partial Q^2} \int_0^\infty dr r (g_\beta(r)f_\alpha(r) + g_\alpha(r)f_\beta(r)) \\ \times \int_\Omega d\cos\theta d\phi e^{i\sqrt{Q^2}r\cos\theta} C_\beta Y_{l_\beta 0}(\theta, \phi) C_\alpha Y_{l_\alpha 0}(\theta, \phi), \quad (57)$$

where l_β and l_α are the orbital quantum numbers of the intermediate states β and α , respectively.

The result for the Q^2 -dependence of the helicity amplitude $A_{1/2}(Q^2)$, when truncating the quark propagator to the ground state, is indicated in Fig. 2. Thereby, we also list the individual contributions of the different diagrams of Fig. 1, which add up coherently. The leading order three quark diagram dominates the prediction for $A_{1/2}$, whereas meson cloud corrections add about 30% to the total result. Here, both the meson-in-flight and the meson-cloud diagrams give the largest contribution. In a next step we include the intermediate excited quark states with quantum numbers $1p_{1/2}$, $1p_{3/2}$, $1d_{3/2}$, $1d_{5/2}$, and

$2s_{1/2}$, that is excitations up to $2 \hbar\omega$, in the propagator. The resulting effect on $A_{1/2}$ is given in Fig. 3. We explicitly indicate the additional terms, which are solely due to the excited states, whereas the ground state propagator result is contained in the curve denoted by TOTAL(GS). Although higher lying state contributions are suppressed relative to the ground state one, they still have a noticeable effect on $A_{1/2}$ for $Q^2 < 0.5 \text{ GeV}^2$ at the order of 15%. For completeness we give the full result for both transverse helicity amplitudes $A_{1/2}(Q^2)$ and $A_{3/2}(Q^2)$ in Fig. 4. The amplitudes fulfil the relation $A_{3/2}(Q^2) = \sqrt{3}A_{1/2}(Q^2)$ for all Q^2 values.

Recently, in the framework of large- N_c QCD [3] it was shown that the ratio $A_{3/2}/A_{1/2}$ is mostly saturated by the naive SU_6 quark model result $A_{3/2}/A_{1/2} = \sqrt{3}$ [25]. Deviations from this standard result are due to higher order corrections with $A_{3/2}/A_{1/2} = \sqrt{3} + O(1/N_c^2)$ [3]. We evaluate the helicity amplitudes at one-loop or equivalently to the order of accuracy $o(1/F^2, \hat{m}, m_s)$, where $F \sim \sqrt{N_c}$. Therefore, to get a nontrivial deviation from the SU_6 result the formalism has to be extended up to two loops or up to order $O(1/F^4) \sim O(1/N_c^2)$. The standard relation between the helicity amplitudes obtained here, which is consistent with large- N_c considerations, is for example not present in the cloudy bag model [11–13]. Latter model, which is conceptually close to our approach, uses in the calculation of one-loop diagrams non-degenerate nucleon and delta masses. This would correspond in our counting scheme to the order of accuracy $O(1/F^4)$, although the complete diagrams to this order are not evaluated. Based on the arguments of the large- N_c analysis it is not surprising that the cloudy bag is able to generate a deviation from the $\sqrt{3}$ result and hence produces a non-vanishing $E2/M1$ ratio.

For comparison with data we turn to the results for the helicity amplitudes at the real-photon point with $Q^2 = 0$. In Table I we list the numerical values for the complete set of Feynman diagrams, again indicating separately the contributions of ground and excited states in the quark propagator. Comparison of our results to other model calculations are presented in Table III. Our final results for $A_{1/2}(Q^2 = 0)$ and $A_{3/2}(Q^2 = 0)$ are in rather decent agreement with the data. As evident from Table I, meson cloud corrections play a decisive role in explaining the large deviation from the result of the impulse, that is three-quark core, approximation. Pion contributions play the dominant role in the meson corrections as evident from Table III, where we list the individual contributions of the octet mesons to the sizable terms generated by the meson-cloud and vertex-correction diagrams. The suppression of K and η loops is due to the large corresponding meson masses occurring in the denominators. The relative contribution of K and η mesons with respect to π is between 8 – 10% in the amplitude, as can be naively expected from the ratio of meson masses $(m_\pi/m_{K,\eta})^2$ which also is roughly 8%. Also, the improved treatment of the quark propagator by including higher excitations tends at least phenomenologically to be required by the data. Again, to obtain a non-vanishing value for the $E2/M1$ ratio, higher order or two-loop corrections have to be considered.

To complete our set of predictions we also indicate the results for the radiative transition $\Delta^+ \rightarrow p\gamma$. For the decay width as based on Eq. (1) we obtain $\Gamma(\Delta^+ \rightarrow p\gamma) = 0.55 \pm 0.03 \text{ MeV}$. Using the experimental value $\Gamma_{total}(\Delta^+) = 111.2 \text{ MeV}$ for the total decay width, we deduce the branching ratio

$$BR(\Delta^+ \rightarrow p\gamma) = (0.47 - 0.52)\% \quad (58)$$

and in similar fashion for the partial decay branching ratios for helicity 1/2 and 3/2

$$BR_{1/2} = (0.12 - 0.13)\% \text{ and } BR_{3/2} = (0.35 - 0.39)\%. \quad (59)$$

These results are again in good agreement with the experimental data of [2]: $BR(\Delta^+ \rightarrow p\gamma) = (0.52 - 0.60)\%$, $BR_{1/2} = (0.11 - 0.13)\%$ and $BR_{3/2} = (0.41 - 0.47)\%$.

IV. SUMMARY

In summary, we have calculated the transverse helicity amplitudes for the transition $\gamma N \rightarrow \Delta$ in the perturbative chiral quark model. Meson cloud corrections are crucial to explain the magnitude of the helicity amplitudes at the real-photon point. We demonstrated furthermore that in the context of the PCQM excited quark states in loop diagrams play an important role at the level of 15% to fully account for the measurements.

Because at one-loop we work at the order of accuracy $o(1/F^2, \hat{m}, m_s)$ or equivalently at $o(1/N_c)$, a deviation from the standard ratio of $A_{3/2}/A_{1/2} = \sqrt{3}$, consistent with large- N_c arguments [3] cannot be obtained. Hence, we also predict a vanishing value for the $E2/M1$ ratio.

A next step will be to explore the effect of two-loop diagrams on the helicity amplitudes, which could possibly explain the non-vanishing $E2/M1$ ratio. In view of the important role of intermediate excited quark states in loop diagrams, it would be also interesting to check their influence on other baryon observables.

Acknowledgements

K.P. thanks the Development and Promotion of Science and Technology Talent Project (DPST), Thailand for financial support. S.C. acknowledge the support of Thailand Research Fund (TRF, Grant No. RGJ PHD/00165/2541). This work was supported by the Deutsche Forschungsgemeinschaft (DFG) under contracts FA67/25-1 and GRK683.

APPENDIX A: SOLUTIONS OF THE DIRAC EQUATION FOR THE EFFECTIVE POTENTIAL

In this section we indicate the solutions to the Dirac equation with the effective potential $V_{\text{eff}}(r) = S(r) + \gamma^0 V(r)$. The scalar $S(r)$ and time-like vector $V(r)$ parts are given by

$$\begin{aligned} S(r) &= M_1 + c_1 r^2, \\ V(r) &= M_2 + c_2 r^2, \end{aligned} \quad (A1)$$

with the particular choice

$$M_1 = \frac{1 - 3\rho^2}{2\rho R}, \quad M_2 = \mathcal{E}_0 - \frac{1 + 3\rho^2}{2\rho R}, \quad c_1 \equiv c_2 = \frac{\rho}{2R^3}. \quad (A2)$$

The quark wave function $u_\alpha(\vec{r})$ in state α with eigenenergy \mathcal{E}_α satisfies the Dirac equation

$$[-i\vec{\alpha}\vec{\nabla} + \beta S(r) + V(r) - \mathcal{E}_\alpha]u_\alpha(\vec{r}) = 0. \quad (A3)$$

Solutions of the Dirac spinor $u_\alpha(\vec{r})$ to Eq. (A3) can be written in the form [26]

$$u_\alpha(\vec{r}) = N_\alpha \begin{pmatrix} g_\alpha(r) \\ i\vec{\sigma} \cdot \hat{r} f_\alpha(r) \end{pmatrix} \mathcal{Y}_\alpha(\hat{r}) \chi_f \chi_c. \quad (\text{A4})$$

For the particular choice of potential the radial functions g and f satisfy the form

$$g_\alpha(r) = \left(\frac{r}{R_\alpha}\right)^l L_{n-1}^{l+1/2}\left(\frac{r^2}{R_\alpha^2}\right) e^{-\frac{r^2}{2R_\alpha^2}}, \quad (\text{A5})$$

where for $j = l + \frac{1}{2}$

$$f_\alpha(r) = \rho_\alpha \left(\frac{r}{R_\alpha}\right)^{l+1} \left[L_{n-1}^{l+3/2}\left(\frac{r^2}{R_\alpha^2}\right) + L_{n-2}^{l+3/2}\left(\frac{r^2}{R_\alpha^2}\right) \right] e^{-\frac{r^2}{2R_\alpha^2}}, \quad (\text{A6})$$

and for $j = l - \frac{1}{2}$

$$f_\alpha(r) = -\rho_\alpha \left(\frac{r}{R_\alpha}\right)^{l-1} \left[\left(n + l - \frac{1}{2}\right) L_{n-1}^{l-1/2}\left(\frac{r^2}{R_\alpha^2}\right) + n L_n^{l-1/2}\left(\frac{r^2}{R_\alpha^2}\right) \right] e^{-\frac{r^2}{2R_\alpha^2}}. \quad (\text{A7})$$

The label $\alpha = (nljm)$ characterizes the state with principle quantum number $n = 1, 2, 3, \dots$, orbital angular momentum l , total angular momentum $j = l \pm \frac{1}{2}$ and projection m . Due to the quadratic nature of the potential the radial wave functions contain the associated Laguerre polynomials $L_n^k(x)$ with

$$L_n^k(x) = \sum_{m=0}^n (-1)^m \frac{(n+k)!}{(n-m)!(k+m)!m!} x^m. \quad (\text{A8})$$

The angular dependence ($\mathcal{Y}_\alpha(\hat{r}) \equiv \mathcal{Y}_{lmj}(\hat{r})$) is defined by

$$\mathcal{Y}_{lmj}(\hat{r}) = \sum_{m_l, m_s} (lm_l \frac{1}{2} m_s | jm) Y_{lm_l}(\hat{r}) \chi_{\frac{1}{2} m_s} \quad (\text{A9})$$

where $Y_{lm_l}(\hat{r})$ is the usual spherical harmonic. Flavor and color part of the Dirac spinor are represented by χ_f and χ_c , respectively.

The normalization constant is obtained from the condition

$$\int_0^\infty d^3\vec{r} u_\alpha^\dagger(\vec{r}) u_\alpha(\vec{r}) = 1 \quad (\text{A10})$$

which results in

$$N_\alpha = \left[2^{-2(n+l+1/2)} \pi^{1/2} R_\alpha^3 \frac{(2n+2l)!}{(n+l)!(n-1)!} \left\{ 1 + \rho_\alpha^2 (2n+l - \frac{1}{2}) \right\} \right]^{-1/2}, \quad (\text{A11})$$

The two coefficients R_α and ρ_α are of the form

$$R_\alpha = R(1 + \Delta\mathcal{E}_\alpha \rho R)^{-1/4}, \quad (\text{A12})$$

$$\rho_\alpha = \rho \left(\frac{R_\alpha}{R}\right)^3 \quad (\text{A13})$$

and are related to the Gaussian parameters ρ , R of Eq. (14). The quantity $\Delta\mathcal{E}_\alpha = \mathcal{E}_\alpha - \mathcal{E}_0$ is the difference between the energy of state α and the ground state. $\Delta\mathcal{E}_\alpha$ depends on the quantum numbers n and l and is related to the parameters ρ and R by

$$\left(\Delta\mathcal{E}_\alpha + \frac{3\rho}{R}\right)^2 \left(\Delta\mathcal{E}_\alpha + \frac{1}{\rho R}\right) = \frac{\rho}{R^3} (4n+2l-1)^2. \quad (\text{A14})$$

REFERENCES

- [1] L. A. Copley, G. Karl, and E. Obryk, Nucl. Phys. **B13**, 303 (1969).
- [2] K. Hagiwara *et al.*, Phys. Rev. D **66**, 010001 (2002).
- [3] E. Jenkins, X. Ji, A. V. Manohar, Phys. Rev. Lett. **89**, 242001 (2002).
- [4] N. Isgur, G. Karl and R. Koniuk, Phys. Rev. D **25**, 2394 (1982).
- [5] S. S. Gershtein and G. V. Jikia, Sov. J. Nucl. Phys. **34**, 870 (1981) [Yad. Fiz. **34**, 1566 (1981)].
- [6] D. Drechsel and M. M. Giannini, Phys. Lett. B **143**, 329 (1984).
- [7] A. J. Buchmann, E. Hernández, and A. Faessler, Phys. Rev. C **55**, 448 (1997).
- [8] A. J. Buchmann, Z. Naturforsch. **52a**, 877 (1997).
- [9] N. Isgur and R. Koniuk, Phys. Rev. D **21**, 1868 (1980).
- [10] M. M. Giannini, Rep. Prog. Phys. **54**, 453 (1990).
- [11] G. Kalbermann and J. M. Eisenberg, Phys. Rev. D **28**, 71 (1983).
- [12] K. Bermuth, D. Dreschsel, L. Tiator, and J. B. Seaborn, Phys. Rev. D **37**, 89 (1986).
- [13] D. H. Lu, A. W. Thomas, and A. G. Williams, Phys. Rev. C **55**, 3108 (1997).
- [14] Y. B. Dong, K. Shimizu, A. Faessler, Nucl. Phys. **A689**, 889 (2001).
- [15] S. Théberge, A. W. Thomas, and G. A. Miller, Phys. Rev. D **22**, 2838 (1980); Phys. Rev. D **24** (1981) 216.
- [16] E. Oset, R. Tegen and W. Weise, Nucl. Phys. A **426** (1984) 456; R. Tegen, Ann. Phys. **197** (1990) 439.
- [17] S. A. Chin, Nucl. Phys. A **382** (1982) 355.
- [18] T. Gutsche and D. Robson, Phys. Lett. B **229** (1989) 333; T. Gutsche, Ph. D. Thesis, Florida State University, 1987 (unpublished).
- [19] V. E. Lyubovitskij, T. Gutsche and A. Faessler, Phys. Rev. C **64**, 065203 (2001).
- [20] V. E. Lyubovitskij, T. Gutsche, A. Faessler and E. G. Drukarev, Phys. Rev. D **63**, 054026 (2001).
- [21] V.E. Lyubovitskij, Th. Gutsche, A. Faessler, and R. Vinh Mau, Phys. Lett. B **520**, 204 (2001); Phys. Rev. C **65**, 025202 (2002).
- [22] V.E. Lyubovitskij, P. Wang, Th. Gutsche, and A. Faessler, Phys. Rev. C **66**, 055204 (2002).
- [23] J. Gasser, M. E. Sainio, and A. B. Švarc, Nucl. Phys. **B307**, 779 (1988).
- [24] J. Gasser and H. Leutwyler, Phys. Rep. **87**, 77 (1982).
- [25] F. E. Close, An Introduction to Quarks and Partons (Academic Press, New York, 1979).
- [26] R. Tegen and R. Brockmann, Z. Phys. A **307**, 339 (1982).

TABLES

Table I. Contributions of the individual diagrams to the transverse helicity amplitudes for $Q^2 = 0$ (in units of $10^{-3} \text{ GeV}^{-1/2}$). Results for inclusion of ground (GS) and excited states (ES) in the quark propagator are indicated separately.

	$A_{1/2}(Q^2 = 0)$	$A_{3/2}(Q^2 = 0)$
GS quark propagator		
3q-core		
-LO	-69.7 ± 5.9	-120.7 ± 10.2
-NLO	-8.6 ± 1.2	-14.9 ± 2.1
Counter-term	8.2 ± 1.1	14.2 ± 1.9
Meson-cloud	-16.7 ± 2.6	-28.9 ± 4.5
Vertex-correction	-0.7 ± 0.1	-1.2 ± 0.1
Meson-in-flight	-23.0 ± 3.4	-39.8 ± 5.9
Total(GS)	-110.5 ± 0.3	-191.3 ± 0.5
ES quark propagator		
NLO	-10.3 ± 1.1	-17.8 ± 1.9
Counter-term	4.9 ± 0.6	8.5 ± 1.0
Meson-cloud	-13.5 ± 2.5	-23.4 ± 4.3
Vertex-correction	-0.7 ± 0.1	-1.2 ± 0.1
Total(ES)	-19.6 ± 3.1	-33.9 ± 5.3
Total=Total(GS)+Total(ES)	-130.1 ± 3.4	-225.2 ± 5.8
Experiment [2]	-135 ± 6	-255 ± 8

Table II. Total result for the helicity amplitudes $A_{1/2}(Q^2 = 0)$ and $A_{3/2}(Q^2 = 0)$ in comparison to other theoretical models (in units of $10^{-3} \text{ GeV}^{-1/2}$). The cloudy bag model results are taken from the values at a typical bag radius $R = 0.8 \text{ fm}$.

	$A_{1/2}(Q^2 = 0)$	$A_{3/2}(Q^2 = 0)$
NRQM [7]	-90.9	-181.9
Cloudy bag model [13]	-128	-222
Relativistic quark potential model [14]	-147	-277
PCQM	-130.1 ± 3.4	-225.2 ± 5.8
Experiment [2]	-135 ± 6	-255 ± 8

Table III. Absolute contributions of π , K , and η to $A_{1/2}(Q^2 = 0)$ for the meson-cloud (MC) and vertex-correction (VC) diagrams in units of $10^{-3} \text{ GeV}^{-1/2}$.

	$A_{1/2}(\pi)$	$A_{1/2}(K)$	$A_{1/2}(\eta)$	Total
GS quark propagators				
MC	-15.3	-1.4	-	-16.7
VC	-0.73	-	0.06	-0.67
ES quark propagators				
MC	-12.4	-1.1	-	-13.5
VC	-0.80	-	0.08	-0.72

FIGURES

Fig.1: Diagrams contributing to the transverse helicity amplitudes: 3q-core (1a), counter term (CT) (1b), meson-cloud (MC) (1c), vertex-correction (VC) (1d), and meson-in-flight (MF) diagram (1e).

Fig.2: Q^2 -dependence of the transverse helicity amplitude $A_{1/2}(Q^2)$ for the case where the quark propagator is truncated to the ground state (GS) contribution. Legend: [3q-LO] - 3q-diagram (leading order); [3q-NLO(GS)] - 3q-diagram (next-to-leading-order); [CT(GS)] - counter term; [MC(GS)] - meson-cloud diagram; [VC(GS)] - vertex-correction diagram; [MF] - meson-in-flight diagram; Total(GS) - total result.

Fig.3: Same as Fig. 2 but now for the case where excited quark states (ES) are included in the loop diagrams. Legend: [Total(GS)] - total result for the ground state quark propagator; [3q-NLO(ES)] - excited states in the 3q-NLO diagram ; [CT(ES)] - counter term; [MC(ES)] - meson cloud diagram; [VC(ES)] - vertex correction diagram; Total = Total(GS)+3q-NLO(ES)+CT(ES)+MC(ES)+VC(ES) - total result.

Fig.4: Total result for the transverse helicity amplitudes $A_{1/2}(Q^2)$ and $A_{3/2}(Q^2) = \sqrt{3}A_{1/2}(Q^2)$.

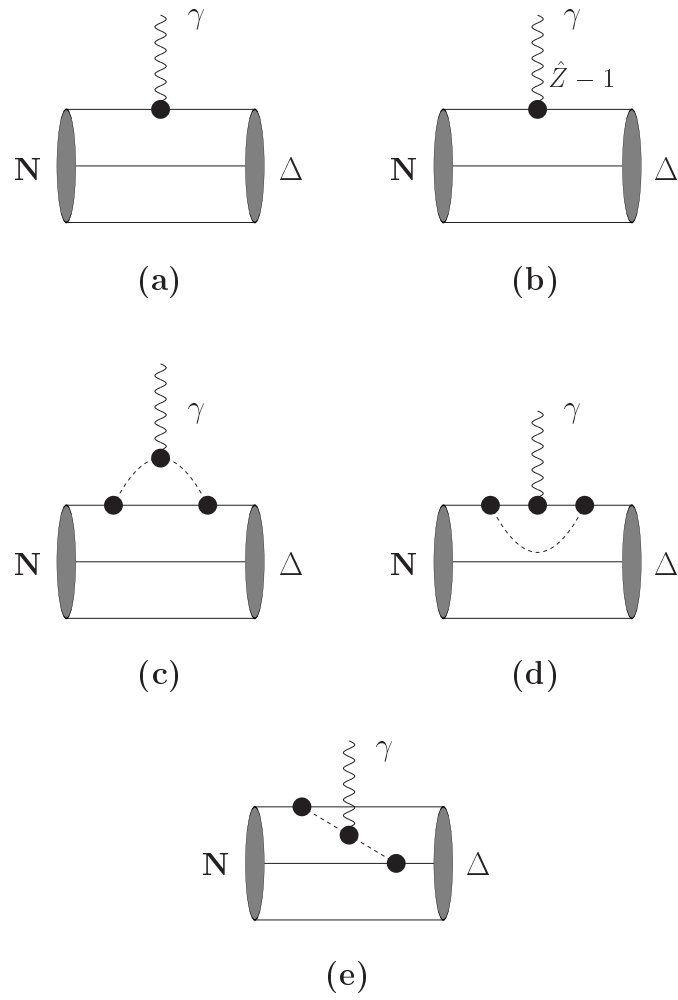


Fig.1

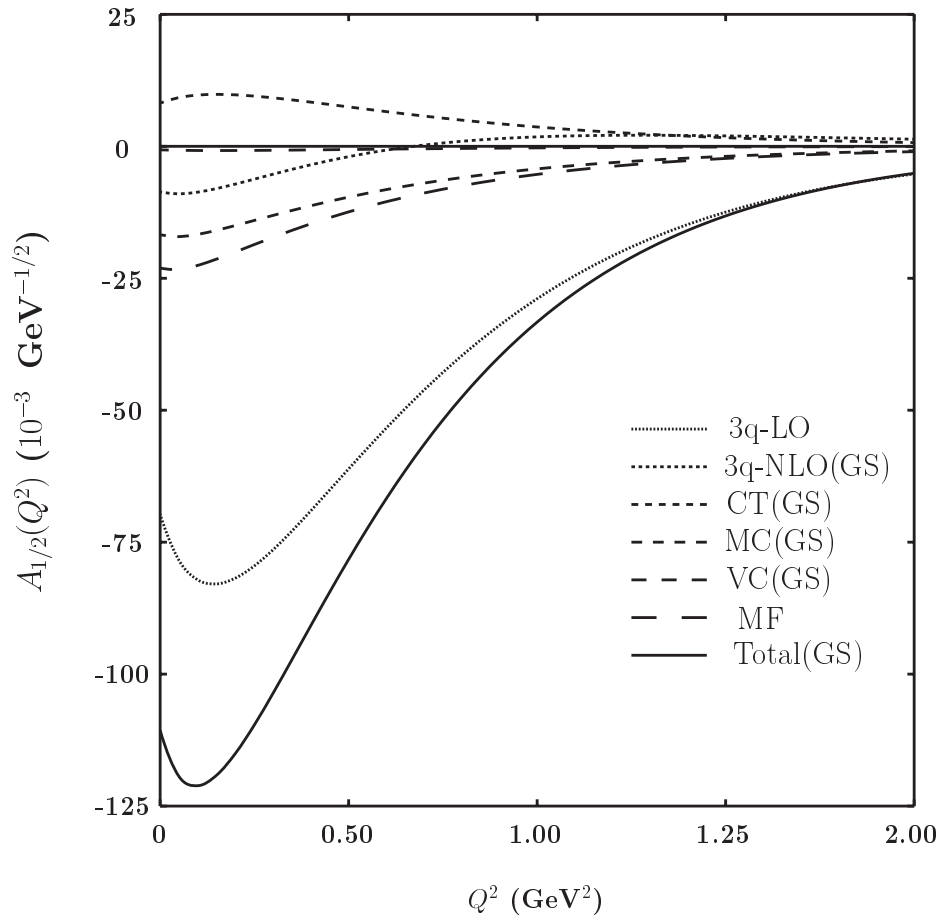


Fig.2

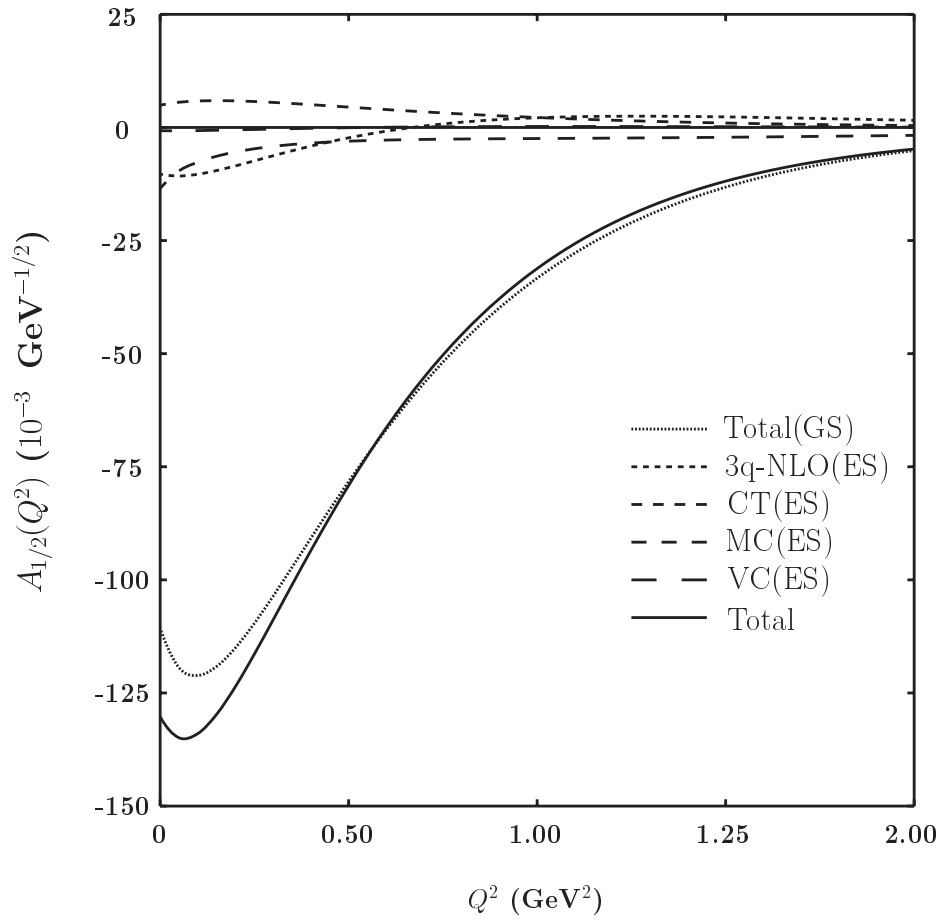


Fig.3

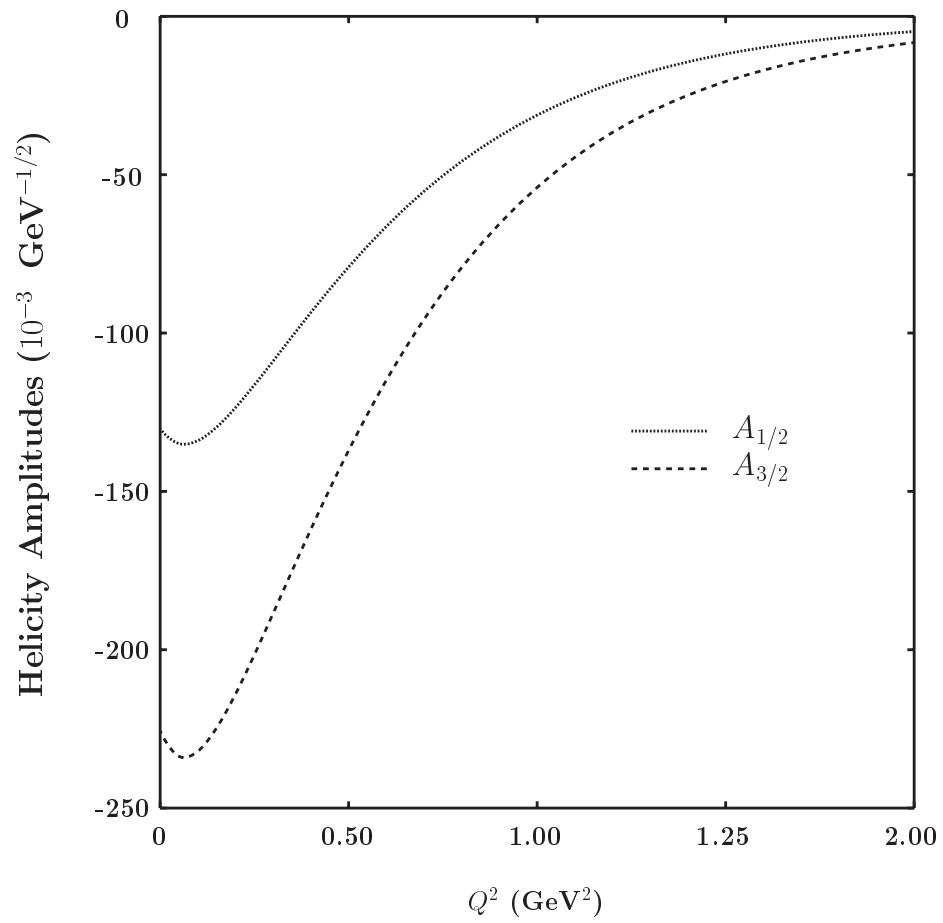


Fig.4